

Research Paper

# Experimental Study and Numerical Simulation of Cutting and Tearing of Silicone Rubber using Extended Finite Element Method

Marwa Gzaïel<sup>1</sup>, Ennouri Triki<sup>2</sup>, Abdelwahed Barkaoui<sup>3</sup>

<sup>1</sup> Laboratoire de Systèmes et de Mécanique Appliquée (LASMAP) Ecole Polytechnique de Tunis, Université de Carthage 2078, La Marsa, Tunisia

<sup>2</sup> Vestechpro, Apparel research and innovation center, 7000 Rue Marie-Victorin, Montréal, QC H1G 2J6, Canada

<sup>3</sup> Laboratoire des Energies renouvelables et des Matériaux Avancés (LERMA), Université Internationale de Rabat, Morocco

Received November 06 2023; Revised February 16 2024; Accepted for publication February 17 2024.

Corresponding author: A. Barkaoui (abdelwahed.barkaoui@uir.ac.ma)

© 2024 Published by Shahid Chamran University of Ahvaz

**Abstract.** Failure of soft materials is a fundamental challenge due to the strongly nonlinear and dissipative deformation involved. An experimental and extended finite element study of dynamic crack in silicone rubber are investigated. Hence, material preparation procedures, details of sample as well as testing apparatus which have been used for cutting, pure shear tests are presented. First, the rate of energy restitution and an instantaneous propagation speed were achieved. The crack propagation speed / energy release rate relationships are given for the different strain rates. Second, an analysis of the mechanical fields and stress state in the fracture process zone is proposed. Finally, cutting force evolution according to stretches is established. Then, an energy-based approach was introduced. Results show that the cutting force and the total cutting energy decreases significantly with increasing deformation rate.

**Keywords:** Silicone, fracture, friction, crack propagation, XFEM, experimental study.

## 1. Introduction

Elastomer material is used in large number fields of applications. The ability of elastomers to withstand very large elastic deformations before breaking makes them the materials of choice in applications combining large deformations and resistance to fracture. Elastomers are frequently used in industrial and medical applications. In particular, silicone rubber is being increasingly used in bio-medical applications owing to their good bio-compatibility (Rochow [1]) (Meunier et al. [2]). However, when used as swollen or stretched membranes, the sudden introduction of crack initiation can lead to catastrophic failure of the structure (Corre [3]). This fracture occurs by the high-speed propagation of one or more cracks.

Since the 1970s, silicone rubber has been indicated for recording preparations for fixed prosthetic restorations. These are natural or synthetic polymers, having a low modulus of elasticity at room temperature and supporting reversible elongations without damage. Due to their wide variety of presentation, they offer many options of use to adapt to different clinical indications (Badr et al. [4]). Take, for example, the making of dental impressions (Chauvel and Turpin [5]).

Silicone rubber is a remarkable material. Although its stability and flexibility, the silicone chain is weak, which means that it tears easily (Bonsor and Pearson [6]). One of the main disadvantages of silicone rubber is its low tear resistance. It can be improved with the addition of other ingredients, but it does not naturally offer resistance to mechanical aggressors (surgical blades, medical probes), resistance to abrasion or resistance to stress (removal of mouth, casting plaster, etc.); so, the application should be carefully evaluated for the suitability of silicone as a solution (Chauvel and Turpin [5]). This problem remains a current topic of research. Indeed, its modeling puts theoretical and numerical models to the test before the need to add dynamics and large deformations to the fracture problem. Therefore, to obtain a reliable and resistant working model, the examination of the impression requires knowledge of the physiology of anatomical structures and mechanical knowledge (fracture, tear, etc.) materials used. Thus, control of their mechanical properties, namely elastic rigidity and fracture toughness.

Based on the fracture mechanic theory, many researchers have therefore developed experimental studies and comparative finite element modeling of silicone rubber (including tear and cutting). For instance, Lake and Yeoh [7] developed a method for assessing the resistance of rubbers to cutting by sharp objects in the absence of friction. They used two forms of test piece (One of the forms is pure shear). The pure shear test piece consisted of a strip of rubber containing a crack parallel to its long edges and it is clamped along these edges and deformed. Then, it had been cutting by a sharp blade. This method extracted results under conditions where there is no effect of friction and independent of test piece shape or size. Thus, results are determined only by the intrinsic properties of the material and the sharpness of the blade. Lake and Yeoh [7] showed that behaviour at low tearing energies obeyed the criterion that the total energy required, from both the deformation of the rubber and the force applied to the blade, was constant.



Afterwards, an experimental steady state of cutting was investigated using a sharp thin blade for soft and glassy polymers (Spagnoli et al. [8]). This method tracking the insertion force versus the penetration displacement. taking the case of soft and highly deformable polymers, Spagnoli et al. [8] were used polystyrene and silicone as materials of experience. Authors were taken into account the influence of large deformations at the crack tip and through full-field finite strain maps obtained by means of digital image correlation. Results showed that the large deformation determines the fracture behaviour when the crack tip is reached by the blade.

In addition, Meunier et al. [2] [9] studies the mechanical behavior of an unfilled silicone rubber. Initially, silicone samples were subjected to several homogeneous tests: traction, pure shear, compression, plane strain compression tests. A finite element simulation and experiment tension test of silicone sample were carried out. During the tests, measurements of the stress field at the surface of deformed samples were obtained. This could be fundamental for crack tip analysis.

Moreover, Baumberger et al. [10] [11] presented an experimental study of the mode I slow and stable crack dynamics in gelatin gels in water/glycerol mixtures. In this model, increasing solvent viscosity slows down cracks, as well, soaking with solvent notably increases gel fragility. Finally, adjusting the viscosity by adding a miscible liquid affects crack propagation by diffusive invasion of the vicinity of the crack tip. The results show that the fracture occurs by viscoplastic tearing of the chain. Therefore, this mechanism, along with the associated phenomenology, should be common to all reversibly cross-linked gels.

Furthermore, Corre [3] developed an experimental study by measuring mechanical fields during the high-speed propagation of a crack in an elastomer polyurethane. The experimental test takes place in two stages, the pretention of the sample then the propagation will take place after induced crack initiation. Each being recorded by a different camera. Monitoring the test involves two cameras, one of which is recorded at high frequency to monitor the propagation. Crack propagation takes place after initiation by a blade in a pre-tensioned membrane. The mechanical approach adopted is based on the measurement or estimation of experimental full fields (displacement field, deformation field and velocity field), in order to analyze a test as the result of a digital simulation. A global energy approach has been developed in which the measurement of fields also makes it possible to make the link between the experiment and the theory at the scale of the influence zone of the crack tip. The rate of energy restitution was associated with an instantaneous propagation speed throughout the propagation. This result confirmed the relevance of the approach consisting in measuring the couple (velocity (V); energy (G)) and using the curve obtained at variable speed.

On the other hand, Triki et al. [12] proposed an energetic approach, based on the application of a pre-strained sample during the combined puncture and cutting test in order to eliminate the contribution of friction. As a result, they showed that for an applied pre-strain energy (i.e., tearing energy) of high value, the friction between the pointed blade and the material was completely eliminated. Therefore, without friction, the total fracture energy was constant. In this case, the contribution to crack growth of the pre-strain energy is spontaneously applied. The growth of the crack was therefore entirely caused by the puncture/cutting by a pointed blade. Finally, the results revealed that the value of the fracture energy corresponding to the perforation/cutting by pointed blades is obtained without friction contribution, but with the presence of the tearing energy contribution.

In this context, and for a better understanding of the mechanics of silicone rubber, failure mechanisms in relation to cutting by razor blade and tearing were investigated. The purposes of this article are (i) to characterize and understand the mechanical behavior of silicone rubber under various mechanical loading (cutting with stretching and tearing tests), (ii) to analyze a total cutting energy technique: an energy balance joined with an instantaneous propagation velocity throughout crack propagation and (iii) to characterize mechanical fields (displacement fields). Concurrently, Using the XFEM and experimental study, we present an investigation of V-dependent energy, mechanical fields and stress states during the propagation of the crack in the silicone elastomer.

## 2. Materials and Methods

### 2.1. Experimental

#### 2.1.1. Material and blades

Elite double is a range of addition silicones (also called polyvinylsiloxans) which come in the form of a base and a catalyst. This range was used for the duplication of models for the dentist's workshop. The polyvinylsiloxane silicones from the Zhermack range are used to manufacture our samples with 32 Shore A (Fig. 1(a)). We mixed liquid of a base component with its crosslinker in equal portions, which hardens after 30 minutes. These elastomers crosslink at room temperature of 25°C under the action of a catalyst generally containing a tin salt. Indeed, sample shape was carried out by molding. This aluminum mold consists of a hollowed lower plate, and a complementary upper plate, allowing the molding of rectangular membrane with dimensions of 100×36×3 mm<sup>3</sup> (Fig. 1(b)).

The razor blade is the Home Planet Gear type, model B08FW6CYG5, from the American Safety Razor Co. The blade is made of steel and 40 millimeters in length, 19 millimeters in width and 0.5 ± 0.05 mm in thickness.

#### 2.1.2. Cutting test by a razor blade with stretching of the sample

An experimental setup was developed to perform cutting tests by a razor blade in the absence of friction (Figs. 1(c) and (e)). i.e., in this method, the stretched sample assumes a V-shape during cut. Subsequently, the edges of the blade will not be in contact with the lips of the membrane. The experimental device is composed of two structures; the INSTRON testing machine supplemented by an ultra-fast scientific camera dedicated to any fields analysis (materials, microscopic phenomena, etc.).

The sample was positioned vertically and clamped between two clips in a mechanical test frame (INSTRON) equipped with a 100 N load cell, as shown in Fig. 1(d). The razor blade was positioned perpendicularly to the sample and moved down at a displacement rate of 60 mm/min. The sample is stretched until reaching the prescribed stretch ratio. Then the blade was inserted directly to cut the membrane with velocity of 60 mm/min. This test makes it possible to characterize the cutting force ( $F_{cut}$ ) for different stretches (from 4% to 50%).

As a result of this experimental study, it was observed how the silicone rubber was deformed by the desired quantity  $\lambda$ . In this process, the sample is spread out. The resulting crack advance is recorded by a camera device (Figs. 1(f) and (g)).

#### 2.1.3. Tear test

In this method, before performing the test, a V-shaped notch is made in the center of the sample. During the test, the two membrane holders are fixed by two pneumatic grips of the INSTRON machines. The camera device is still superimposed for shooting during tear testing (Fig. 1(a)).

The aim was to determine the average crack propagation speed for different stretches (7%, 8%, 10%, 15% and 20%). It was calculated by dividing the displacement of the crack, measured from the images provided by the cameras, by travel time.

Tear tests in the absence of friction and without sliding of the blade were carried out. The test duration has been presented in Fig. 2.



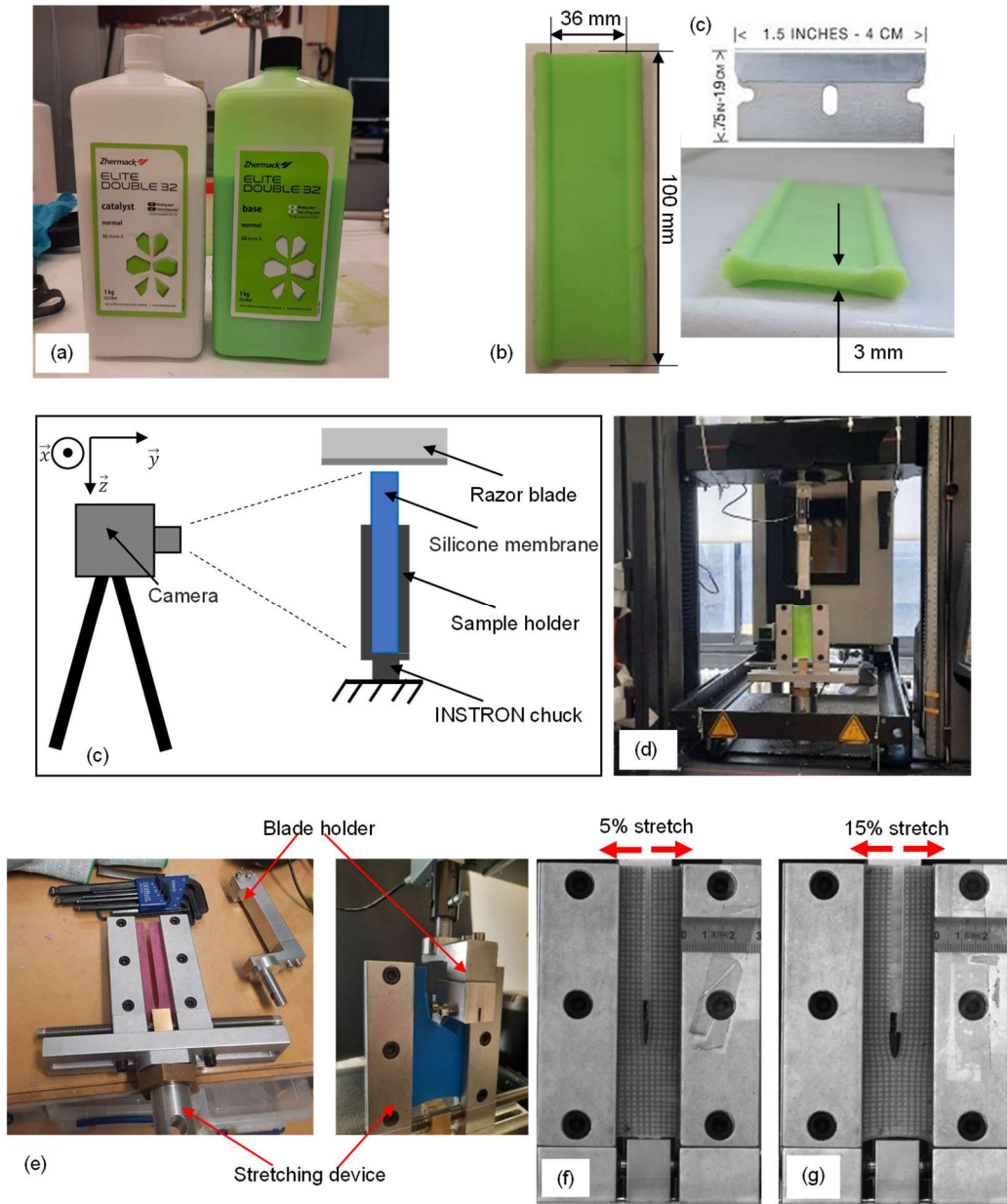


Fig. 1. (a) Zhermack Double 32. (b) Sample of the silicone membrane. (c) Experimental fracture protocol of a 3 mm thick silicone membrane. (d) Experimental set-up of cutting with razor blade using the INSTRON testing machine. (e) Specimen holder for stretching tests with endless screw. (f) Cutting of the stretched membrane (5% stretch) with a razor blade (thickness 0.5 mm) and a penetration velocity of 60 mm/min. (g) Cutting of the stretched membrane (15% stretch) with a razor blade (thickness 0.5 mm) and a penetration velocity of 60 mm/min.

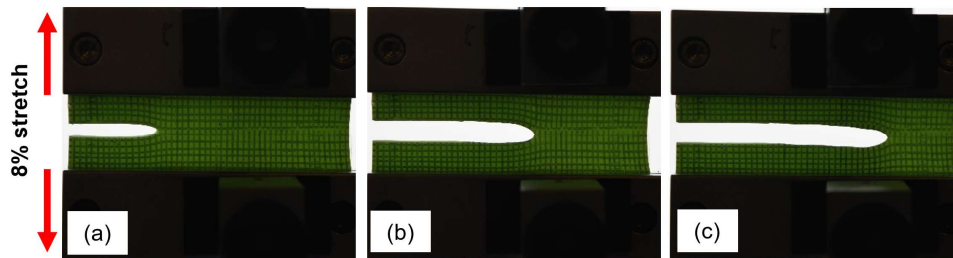


Fig. 2. Crack propagation process of an experimental tear test of the silicone membrane for a stretch of 8% (this figure is captured by camera).

The characterized sample is a piece of silicone, with a 40 mm notch made along its length, to obtain a V-shaped sample. The test takes place in two stages, the pre-tensioning of the sample then the propagation of the crack. As soon as the targeted elongation has been reached, the pre-crack propagates freely. It is specified that the notch is made while the crosshead is still in motion: given the very short duration of this step (between 16 and 300 ms), the crosshead can be considered as fixed throughout the propagation.

2.2. Finite element analysis

The tear test is numerically simulated using the extended finite element method (XFEM) and the ABAQUS (general statics) computer code. This method allows us to model the crack propagation, using cohesive behavior based XFEM approach.



More importantly, using XFEM offers several advantages with regard to the crack itself: Such it is not necessary to specify the path of the crack and its initial location. Also, the mesh is generated independently of the crack and there is no need to partition the geometry at the crack location; even if the mesh density must be high enough (Abaqus [13]).

By reproducing the experimental tear tests, a geometric model of the membrane and the crack was developed with well-defined boundary conditions. To illustrate the principle of XFEM, we used the generic properties of silicone:  $E = 1.092 \text{ MPa}$ ,  $\nu = 0.49$ ,  $\rho = 1000 \text{ kg/m}^3$ . These elastic properties of the materials were obtained through an experimental study carried out in another research project conducted in the same laboratory where we conducted our experiments.

To model crack propagation in Abaqus, it is necessary to describe damage initiation and evolution behaviors.

The maximum principal stress criterion was used (Abaqus [13]). The damage initiation was defined as part of the material properties, using the damage for the Traction Separation laws "Maxps Damage" (equals 5.57 MPa) (Gigliotti [14]).

With this option, the damage can start when the maximum principal stress exceeds the given value. We used the option "maximum displacement" (is equal to 0.001 m) to specify the softening behavior (Abaqus [13]). In the interaction module, initial location of the crack was specified. Finally, the mesh was much simpler, because it is not necessary to partition an initial crack or circular regions around the crack tip. CPS4R bilinear quadratic 4-node elements were used to mesh the model (Fig. 3.).

2.3. Energy calculation

2.3.1. Tearing energy

The presence of dissipative phenomena at the crack tip results in energy consumption during its propagation. This dissipation of energy expressed per unit of surface created is called energy of fracture,  $\Gamma$  (in  $\text{kJ.m}^{-2}$ ). This scalar quantity synthesizes all the physical phenomena taking place at the crack tip. Equivalently, it is sometimes seen as the resistance of the material to crack propagation (Freund [15]). Initially postulated by Griffith [16] in the form of surface energy,  $G_{rupture}$  takes on a broader meaning to apply to different materials; in elastomers, in particular Rivlin and Thomas [17] call it tearing energy, which is written as:

$$G_{rupture} = \omega_0 \cdot \int_1^\lambda \sigma \cdot d\lambda \tag{1}$$

with

$\omega_0$  : The width of the sample,

$\lambda = 1 + \varepsilon$  : Elongation,

$\sigma$  : Cauchy stress tensor.

The strain energy is given by Zhu et al. [18]:

$$W(\lambda) = \int_1^\lambda \sigma \cdot d\lambda \tag{2}$$

Neo-Hookean 's model function is a function allowing to estimate the strain energy related to elongation  $\lambda = 1 + \varepsilon$  (Zhu et al. [18]):

$$W(\lambda) = \frac{\mu}{2} (I_1 - 3) \tag{3}$$

and  $I_1$  is the first invariant of the Cauchy strain tensor as:

$$I_1 = \lambda_1^2 + \lambda_2^2 + \lambda_3^2 \tag{4}$$

and

$$\lambda_1 \cdot \lambda_2 \cdot \lambda_3 = 1 \tag{5}$$

and since the shear is pure,  $\lambda_3 = 1$ ,  $\lambda_2 = 1 / \lambda_1$ .

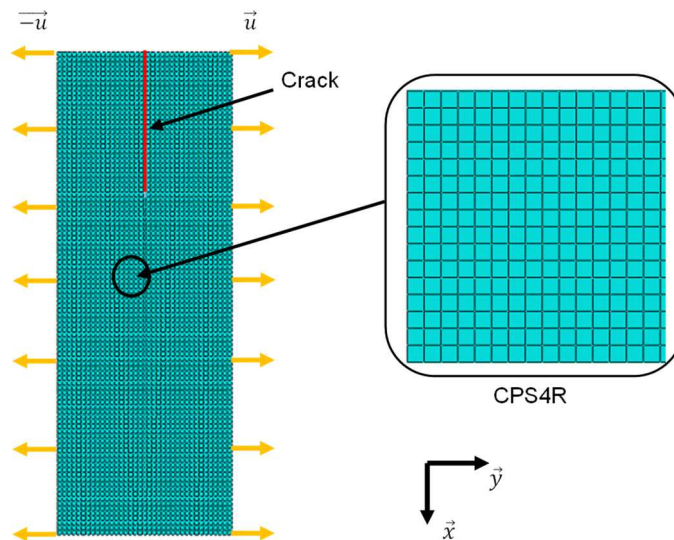


Fig. 3. Finite element model of silicone membrane.



So, Eq. (3) becomes:

$$W(\lambda) = \frac{E}{6} \left( \lambda^2 + \frac{1}{\lambda^2} - 2 \right) \quad (6)$$

Finally, Eq. (1) can be written:

$$G_{rupture} = \omega_0 \cdot \frac{E}{6} \left( \lambda^2 + \frac{1}{\lambda^2} - 2 \right) \quad (7)$$

### 2.3.2. Total cutting energy

According to the energy-based approach proposed by Triki et al. [19], using the theory of Rivlin and Thomas [17], it is allowed to calculate the total cutting energy  $G_{cutting}$  (Eq. (8)). In this method, the force-blade displacement curve was recorded from blade failure into elastomer rubber. The area under each force-blade displacement curve presents the total cutting work ( $U_{Total}$ ). Subsequently, the total cutting energy ( $G_{Total}$ ) was determined by dividing the total cutting work by the fracture surface area:

$$G_{Total} = - \left( \frac{\partial U_{Total}}{\partial A} \right) \approx \frac{\Delta U_{Total}}{\Delta A} \quad (8)$$

where  $\Delta U_{Total}$  denotes the total cutting work that corresponds to the fracture surface variation  $\Delta A$ . According to the razor blade geometry, the fracture surface area was well displayed as a rectangle:

$$\Delta A = t \cdot \Delta x \quad (9)$$

with  $t$ : membrane thickness (mm),  $x$ : razor blade displacement (mm).

## 3. Results and Discussion

### 3.1. Tear test without sliding of blade

The fracture energy is an important fracture property parameter and can directly reflect the crack resistance of this material. In our case, the criterion retained is the energy criterion of Griffith. During crack propagation, the energy dissipated at the tip of the crack is the fracture energy, a quantity linked to the material and a function of the propagation speed only. The application of the criterion of Griffith implies simply that the energy release rate  $G$  is equal at each moment to this energy of fracture (Eq. (7), Corre [3]). To use the formulation of Freund [15], the equation is therefore written in all generality:

$$G_{rupture} = \Gamma \quad (10)$$

This equation is also called the equation of motion of a crack by analogy with point mechanics (Freund [15], Bouchbinder et al. [20]).

Figure 4 plots the variation of the tearing energy  $\Gamma$  calculated by Eq. (10) as a function of  $\lambda$ . It can be seen that the tearing energy  $\Gamma$  increases with stretch values. Subsequently, it is concluded that the greater the material deformation, the easier the fracture of the membrane becomes. In this case, the tearing energy is fully similar to fracture energy at each moment that the crack propagates.

### 3.2. Average velocity of crack propagation

To obtain the velocity of the crack relative to the material, it is necessary to overcome the movements of the membrane. The crack propagation velocity  $V$  is obtained from the division of the variation in the position of the crack tip by time elapsed during this variation (Table 1). Far from the edges of the sample, in this configuration, experience has shown that the cracks run at a constant speed (see Fig. 6 and Table 1). As expected, free edges affect crack propagation up to a distance comparable to the width of the membrane (Fig. 5 (Zone (a) and (c))). Further, data processing was systematically limited to the central region (Fig. 5 (Zone (b))), extending over 40 mm. In this region, it can be legitimately calculating the energy release rate (Baumberger et al. [10, 11]).

Such experiments (nominal deformation < 10%) give rise to executions which take a long time. It is noted that the crack progressed slowly. Beyond 10%, the crack propagated rapidly, noting that for all the tests, crack propagation speed is always constant, as shown in Fig. 6.

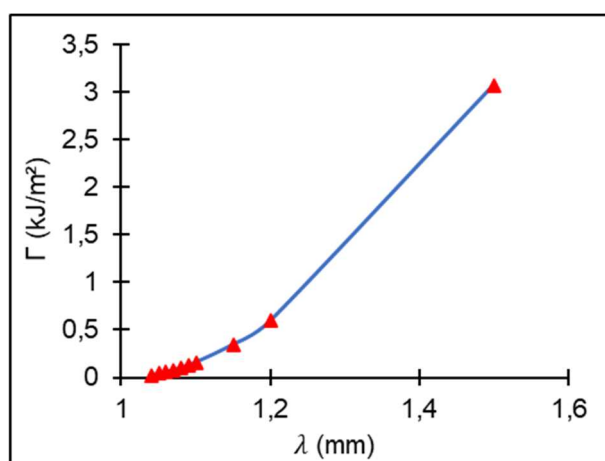


Fig. 4. Variation of energy release rate as a function of  $\lambda$ .



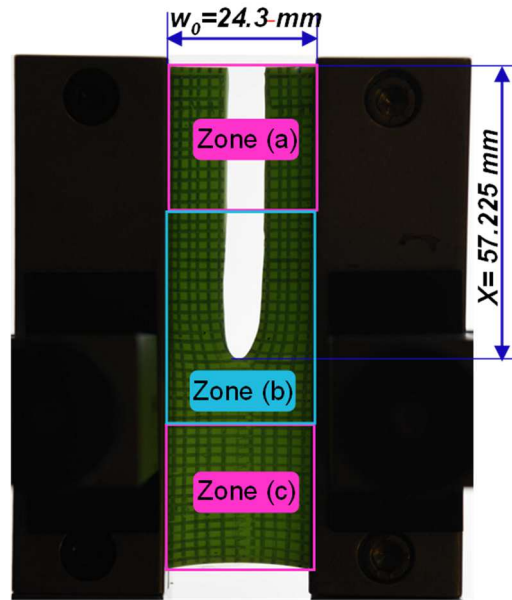


Fig. 5. Example of an experimental tear test of silicone membrane for a stretch of 7% with crack distance of 57.225 mm at a time of 108.748 s.

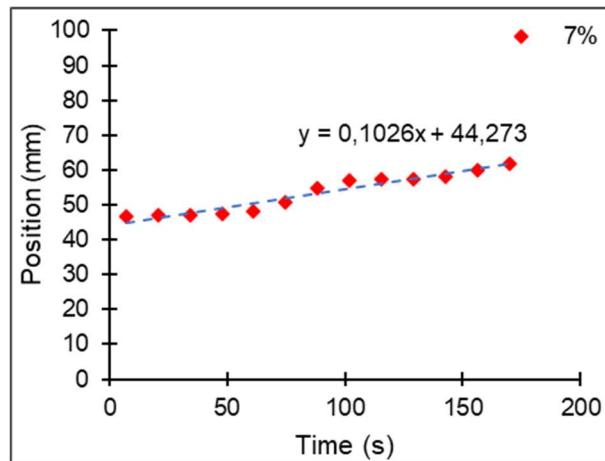


Fig. 6. Experimental crack position as a function of time for the nominal strain 7%.

### 3.3. Variation of $\Gamma$ with propagation velocity ( $V$ )

For an arbitrary crack propagation, the detailed knowledge of the trajectory of a crack requires adding an ingredient to the mechanics of continuums: a propagation criterion. The criterion used is the energy criterion of Griffith [16]. During crack propagation, the energy dissipated at the tip of the crack is the fracture energy  $\Gamma(V)$ , a quantity related to the material and a function of the propagation speed  $V$ . The application of the Griffith criterion simply implies that the rate of energy restitution  $\Gamma$  is equal at each instant to this energy of fracture. The pure shear sample makes it possible to impose the energy release rate by controlling the deformation of the sample. The uniqueness of the curve  $\Gamma(V)$  validates the hypothesis of fracture energy as the mechanical quantity characteristic of fracture (Freund [15]). Likewise, the determination of the curve  $\Gamma$  as a function of  $V$ , which is necessary for the prediction of crack growth, is supposed to be a material parameter for a given elastomer (Greensmith and Thomas [21]).

Figure 7 shows the evolution of the energy release rate as a function of the crack propagation velocity in the deformed configuration. Energy values are calculated by the analytical formula (stationary propagation) mentioned in section 2. As seen in Fig. 7,  $\Gamma$  is highly dependent on the crack propagation rate.  $\Gamma(V)$  becomes noticeably steeper as  $\lambda$  increases. Williams et al. [22] indicated that the effects of propagation velocity on the rate of energy restitution  $\Gamma$  for a dynamic crack follow the viscoelastic behavior predicted by the WLF relationship. The fracture energy therefore increases with the propagation velocity. The velocity dependence is due to the large viscoelastic dissipation contribution of the material (Gzaiel et al. [23]).

Referring to Gzaiel et al. [23] and Persson et al. [24], Fig. 7 shows two different fracture regimes related to the crack propagation velocity. In the first regime A (Fig. 7), at low deformation strain,  $\epsilon < 10\%$ , the energy release rate  $\Gamma$  reached a plateau independent on the propagation velocity, the fracture of material can be considered as an elastic solid fracture and  $\Gamma = \Gamma_0$ .  $\Gamma_0$  is called the threshold at  $0.1 \text{ kJ/m}^2$  for which the tearing of the networks begins. In the second regime B (Fig. 7),  $\epsilon > 10\%$ ,  $\Gamma$  increases in a linear fashion with the velocity.

Table 1. Experimental values of the crack propagation velocity as a function of the nominal strain.

Nominal strain (%)	7	8	10	15	20
Average velocity (mm/s)	0.1028	0.2737	288.7	779.41	1486.9



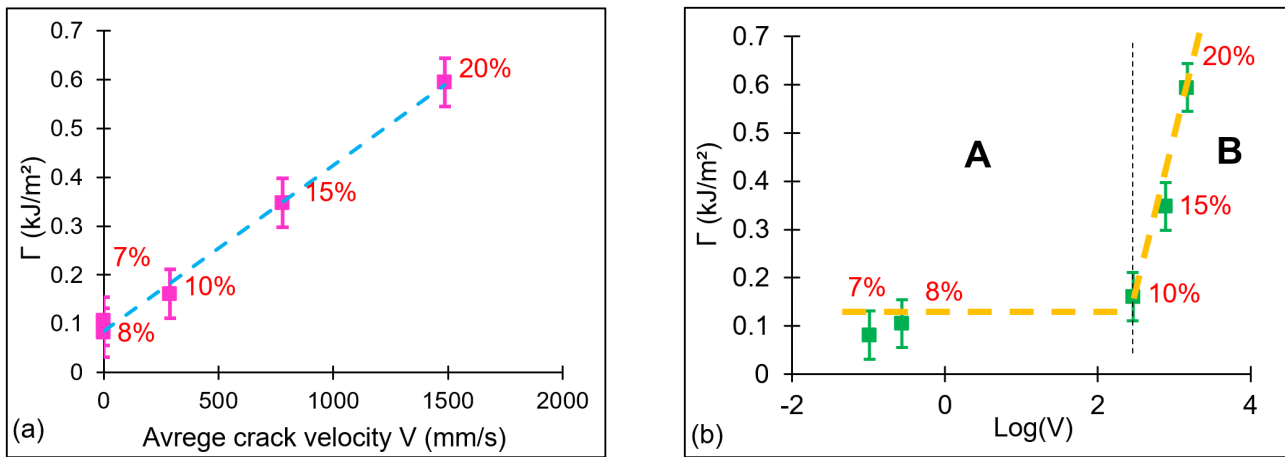


Fig. 7. Evolution of the energy release rate during dynamic propagation in silicone rubber (pure shear sample) as a function of the average crack speed. (a) Gross results. (b) Modified plot with  $\log(V)$ .

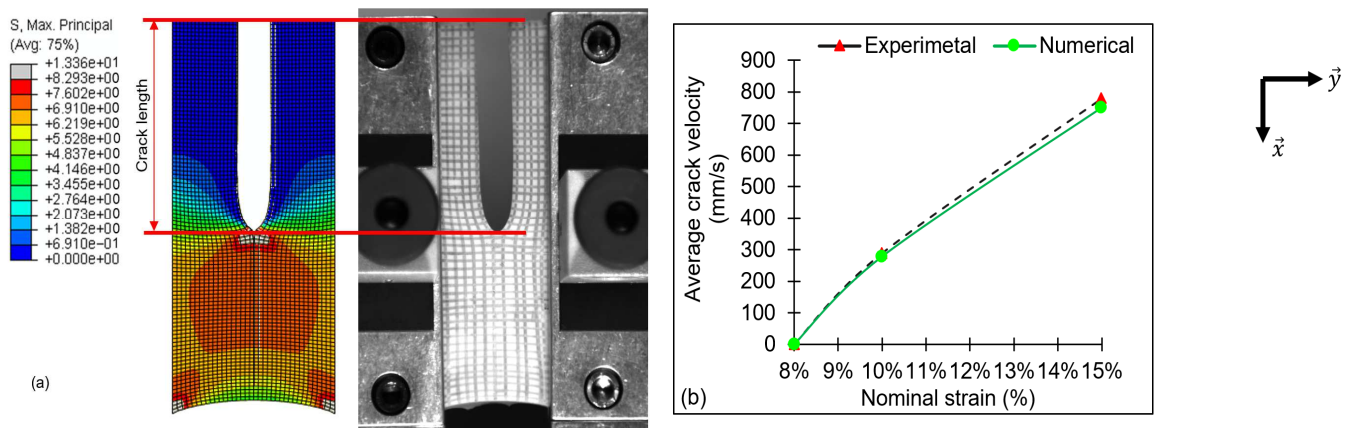


Fig. 8. (a) Crack length in the experiment and numerical model. (b) Experimental and numerical variation of the average crack velocity vs the nominal strain.

### 3.4. FE model validation

The deformed shape and crack velocity characteristics were used to validate the proposed model. For validation purposes, a tear experiment was carried out. A visual comparison between the actual and numerical deformed shape is shown in Fig. 8(a). This comparison allows observing the crack position and making the calculation of crack propagation speed easier. As can be seen, the deformation characteristics in the model are very similar to those of the experiment. Figure 8(b) gathers steady-state crack velocity obtained for various samples and different prescribed stretch ratios  $\lambda$  for both the numerical and experimental test. To provide a more quantitative comparison, the crack velocity in the experiment and numerical model are plotted in Fig. 8(b). As can be seen, good agreement was obtained, thus providing confidence in the model. The proposed model was considered to have been validated and sufficiently accurate to proceed showing and examining mechanical fields.

### 3.5. Local mechanical fields

In the previous section, each crack propagation test provides the global scalar quantities: a stabilized speed, the associated energy release rate, the elongation of the membrane, the opening angle. We complete the results that showed the maintenance of this continuous relationship between the speed of propagation and the rate of energy restitution during the same steady propagation through the examination of mechanical fields.

To illustrate the method and allow comparability, displacement field shown in this section is issued from a test with a stretch ratio of 10%. The instant chosen corresponds to the pictures in Fig. 9 where the crack speed is growing at  $277.52 \text{ mm s}^{-1}$ . In addition, sample sizes are indicated by the vertical and horizontal axes, graduated in mm. XFEM Method is based on the measurement of displacement field. As an example, Fig. 9 shows the displacement field ( $x = 4.6 \text{ mm}$ ) in the deformed configuration. The knowledge of the field of displacement makes it possible to calculate the position of the crack tip and to follow the evolution of crack propagation at each node of the mesh, thus helping to make easier the calculation of crack propagation velocity.

### 3.6. Stress state analysis

In this section, the relationship between the stress state and the applied stretches is determined. A finite element analysis was performed to evaluate the stress state involved at several applied deformation during the tear simulation of 3 mm thick silicone rubber.

Stephenson et al. [25] have studied the deformations and stresses in a slab of all-around infinite extent containing a traction-free plane crack, under conditions of plane strain. They showed that, for an hyperelastic materials, the finite theory, in contrast to linearized elastostatics (only mode I), predicts that the crack opens in the vicinity of its tips also for a Mode II loading, at least for a certain range of the hardening parameter. As well, in Fig. 10, crack propagation at 10% stretch shows a mixed crack growth as well, which is dominated by the tension fracture Mode I,  $\sigma_{xx} = 9.231 \text{ MPa}$  and  $\sigma_{yy} = 11.46 \text{ MPa}$  (Fig. 10). In addition, crack growth occurs due to shear fracture, given by the shear stress Mode II,  $\tau_{xy} = 6.689 \text{ MPa}$ . These stress values indicate the maximum values on the legend of the stress contour plot in the analysis results.



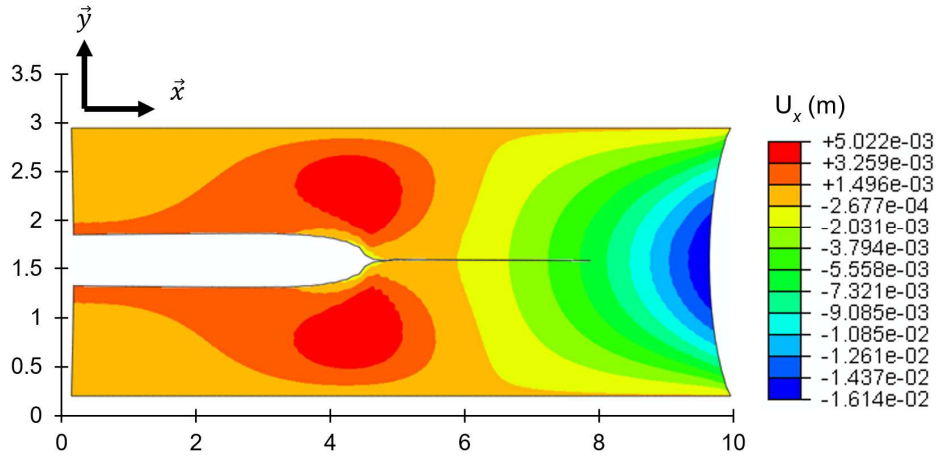


Fig. 9. Contours of horizontal displacement field ( $x = 4.6$  mm) during crack growth in the deformed configuration with 10% deformation strain.

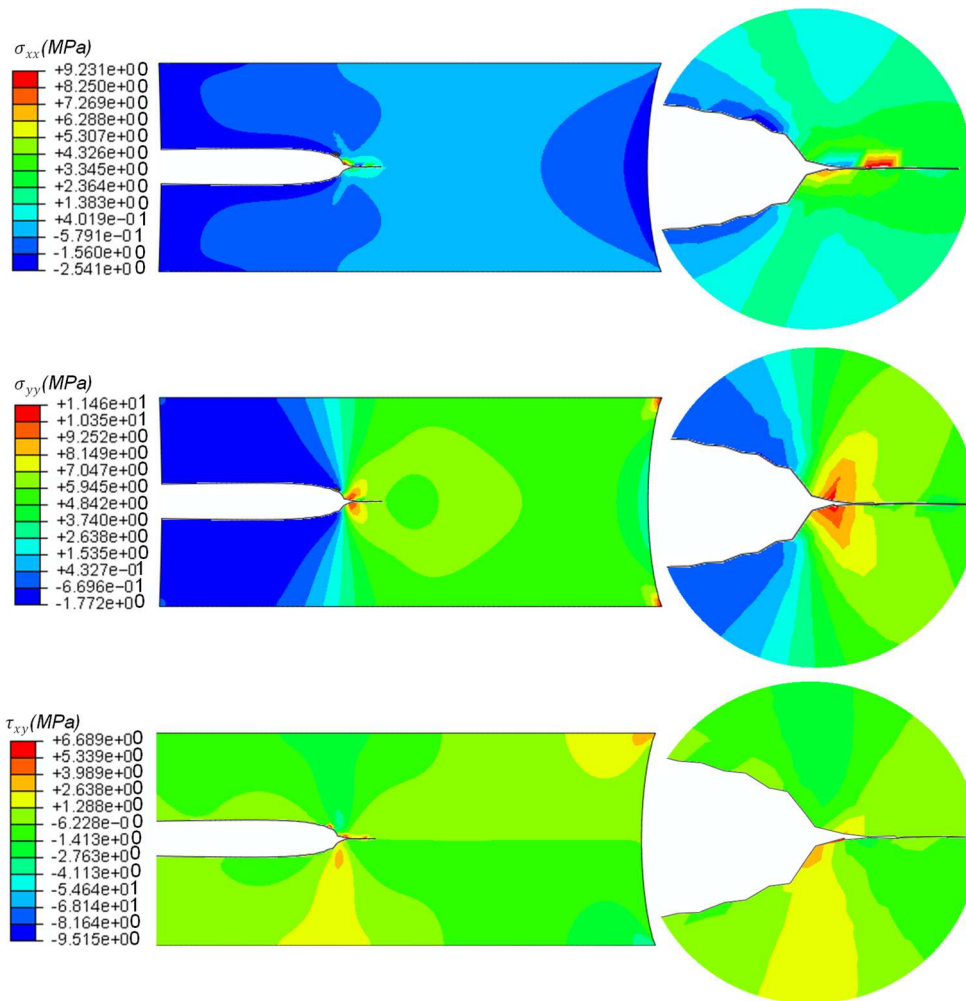


Fig. 10. Contour levels of the stress components during crack growth in the deformed configuration with 10% deformation strain of 3 mm thick silicone rubber.

Therefore, the tear of a 3 mm silicone membrane at 10% stretch illustrated a dominated tension failure (Fig. 10). To understand the crack growth at several stretches, the effect of the applied stretch on the stress field is plotted in Fig. 11. Following results shown in Fig. 11, the stress field should be dependent on the membrane deformation. The results also show how the two fracture modes are involved during crack propagation of silicone rubber. For all stretch values (7%, 8%, 10% and 15%), the crack, resulting from the tear test, is controlled by mixed fracture mode of mode I and mode II. The tension fracture Mode I was given by the tension stresses  $\sigma_{xx}$  and  $\sigma_{yy}$ , while the shear fracture Mode II was given by the shear stress  $\tau_{xy}$ . As can be seen here, an increase in stretch causes an increase in tension stresses ( $\sigma_{xx}$  and  $\sigma_{yy}$ ) and shear stress  $\tau_{xy}$  (Fig. 11). However, this increase is dominated by a uniaxial tension  $\sigma_{yy}$  (Fig. 11), which provides a fracture Mode I.

### 3.7. Combined cutting and tear test by sliding of blade

Figure 12 is a typical example of the information obtained during an experimental cutting test without stretching ( $\lambda = 0$ ) using the INSTRON 100 N Testing Machine. This curve shows the cut force  $F_{cut}$  developed when the blade cuts and penetrates a silicone sample of 3 mm thick at 60 mm/min insertion velocity.



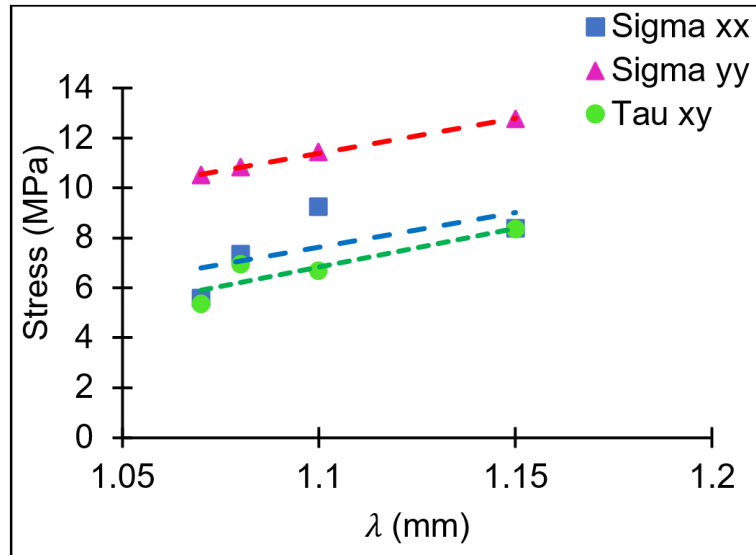


Fig. 11. Stress versus  $\lambda$  variation obtained from tearing of silicone membrane (3 mm thickness).

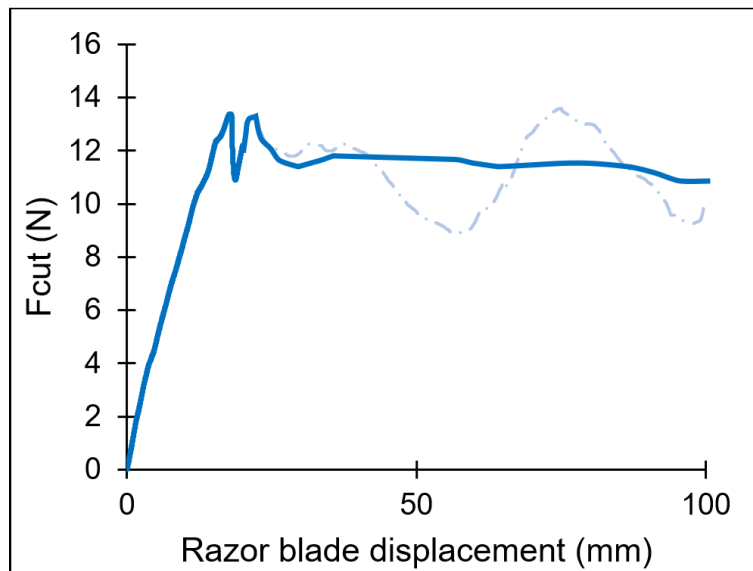


Fig. 12. Cutting force as a function of razor blade displacement during cutting test of 3 mm thick silicone without stretching ( $\lambda = 0$ ).

During blade penetration, the cutting force increases with distance traveled by the razor blade, up to a maximum value equal to 12 N and then reaches a plateau. Vu-Khanh et al. [26] indicated that the spent cutting energy depends, for a large part, on the frictional energy due to the interaction of the sample with the two sides of the blade. The friction energy occurred during the cutting of an elastomer material by a razor blade can be removed, when applying a pre-strain.

Figure 13 ((a) and (b)) illustrates an example of cutting force ( $F_{cut}$ ) and stab cutting force variation respectively as a function of the deformation rate at 60 mm/min insertion velocity, ranging from a stretch of 4 to 50%, applied to silicone membranes of 3 mm thickness. The stab cutting force was the plateau force (when the curve reached a plateau).

In brief, three parts are observed specifically in every curve (Fig. 13(a)). The results analysis showed that in the first part A,  $F_{cut}$  suddenly increases with a strong peak. This peak is explained by the initial cutting process between the blade and the membrane. On the contrary to Fig. 12 ( $\lambda = 0$ ), results show that  $F_{cut}$  decreases continuously with the elongation  $\lambda$  (illustrated in Fig. 13(b)). This outcome is due to the decrease in friction contribution, i.e., when the applied deformation/ or tearing was increased, the frictional contribution decreased.

Indeed, in the second part B (from 9 mm razor blade displacement), the force decreases in a linear fashion with razor blade displacement. This dependent is related to the competition between tear (fracture) and friction contribution. The slight decrease in the cutting force at the beginning of part B can be related to the lateral pressure exerted by the material on the edges of the blade (Vu-Khanh et al. [26]). In addition, the force required to cut the material without friction is very low compared to that with friction (Vu-Khanh et al. [26]). When the friction between razor blade and material is completely removed, there is another factor compelling. In this case, results show that tearing energy had high value. As the applied deformation increases, the tearing energy become dominant and a frictional contribution is moving towards zero.

The signal recorded, after 50 mm razor blade displacement (Part C) (illustrated in Fig. 13(a)), represents the cutting force  $F_{cut}$  since the frictional force is zero. It has been found that the total cutting energy is valid up to an applied deformation  $\varepsilon \leq 15\%$  (Part A' and B'). In part A' ( $\varepsilon \leq 4\%$ ), friction contribution remains greater than that in part B' due to the continued interaction of the sample with both sides of the blade until total cutting test (razor blade displacement = 100 mm). Afterwards, in part B' ( $5\% \leq \varepsilon \leq 15\%$ ), the cutting operation becomes easier; the cutting force decreases, and the friction tends towards zero while increasing tear. Finally, beyond 15% (Part C'), the fracture becomes uncontrolled, and the crack goes faster than the blade.



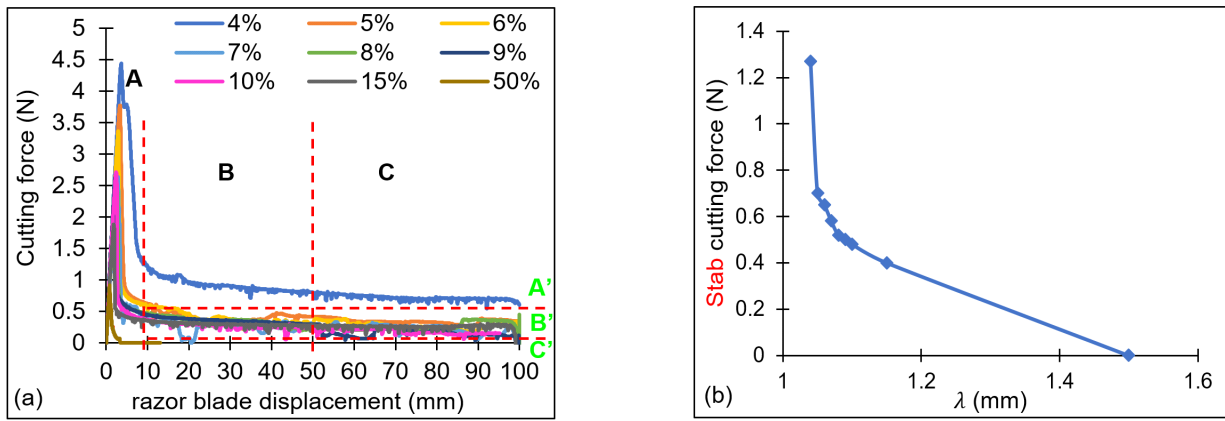


Fig. 13. Combined cutting and tear of silicone membrane (3 mm) by a razor blade at different nominal strain (from 4% to 50%) with insertion velocity of 60 mm/mn. (a) Variation of typical experimental force-displacement curves. (b) Stab-cutting force versus  $\lambda$  variation curve.

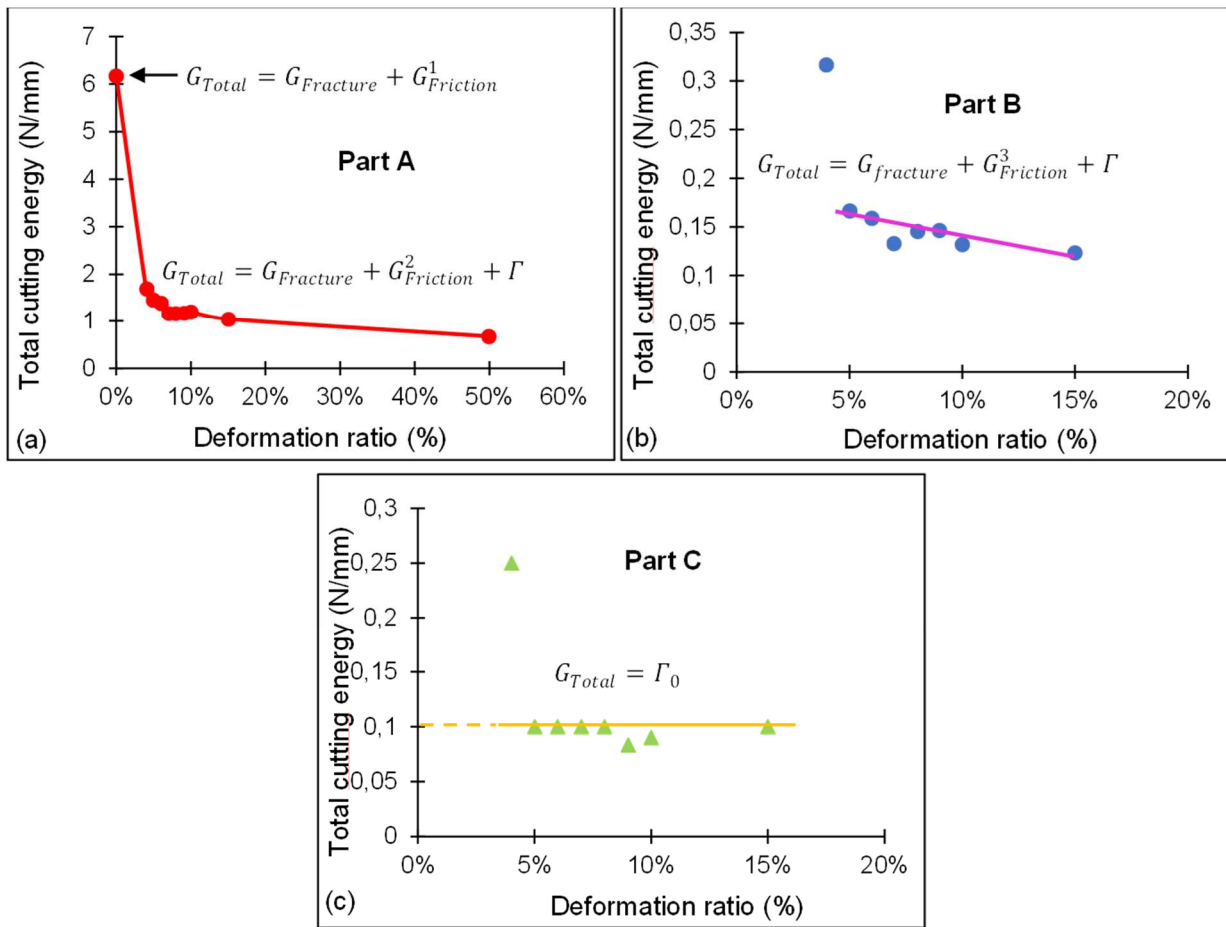


Fig. 14. Variation of  $G_{Total}$  as a function of deformation ratio obtained from the combined cutting and tear test of a silicone membrane (3 mm of thickness) by razor blade. (a) Part A of Fig. 13. (b) Part B of Fig. 13. (c) Part C of Fig. 13.

Combined cutting and tear of silicone rubber 3 mm thick by sliding razor blade was carried out to measure the energies involved during the blade movement in the material. The combined cutting and tear tests were repeated with different stretches of the sample (Figure 13 (a)). Results of Figure 13 (a) were splitted to three parts (shown in Fig. 17). As mentioned earlier, according to the energy-based approach (Triki et al.2017), Fig. 14 illustrates the dependence of the total cutting energy (Eq. (8)) with respect to the applied deformation, in the case of silicone membrane thickness (3 mm), using a razor blade for several values of applied stretches.

Figure 14 plots the variation of Total energy,  $G_{Total}$ , as a function of deformation ratio obtained from the combined cutting and tear test of a silicone membrane (3 mm of thickness) by razor blade.

Combined cutting and tearing experiments of silicone rubber using razor blade was conducted to set an experimental energy-based approach. Results show that the cutting force and the total cutting energy decreases significantly with increasing deformation ratio ( $4\% \leq \epsilon \leq 50\%$ ). As well, the tear energy only contributed to removing friction. As shown in Fig. 14, the total cutting energy decreased from 6.17 to 0.1 kJ/m<sup>2</sup>. In the first Part A (Fig. 14(a)), at  $\epsilon = 0\%$ , the maximum value of total cutting energy  $G_{Total}$  also partly encompasses frictional contribution of over 60% (Triki et al. [27]). Therefore, the total cutting energy given by Eq. (11) that can be written as:



$$G_{Total} = G_{Rupture} + G_{Friction}^1 \quad (11)$$

with,  $G_{Rupture}$ : fracture energy and  $G_{Friction}$ : friction energy.

When the applied stretch was increased ( $\epsilon \neq 0\%$ ) (Fig. 14(a)), the frictional contribution decreased. During this step, the friction energy and the tear energy were both present during the cutting/tear test.  $G_{Total}$  can thus be obtained by Eq. (12):

$$G_{Total} = G_{Rupture} + G_{Friction}^2 + \Gamma \quad (12)$$

Interestingly, the total cutting energy decreases significantly as the applied deformation increases (Fig. 14(b)), while the tear energy increases and the friction energy decreases more and more.

At last,  $G_{Total}$  decreased to reach a plateau leads to a constant value of  $0.1 \text{ kJ/m}^2$  since the increasing of the stretch (Fig. 14(c)). Results shown that  $G_{Total}$  seemed to be substantially unaffected with the applied deformation. Hence, it appears that the frictional contribution is completely removed starting from increasing of applied pre-strain ( $\epsilon \geq 5\%$ ).

A similar trend has been reported in the case of combined puncture and cutting by pointed blade of pre-strain neoprene sample (Triki et al. [12]). Triki et al. [12] have shown that  $G_{Total}$  seemed to be substantially unaffected with tearing energy variation. Furthermore, it appears that the frictional contribution was completely removed starting from increasing of applied pre-strain. Therefore, the applied total fracture energy  $G_{Total}$  was only offered by the intrinsic fracture energy (Triki et al. [12]). Moreover, Persson et al. [24] showed that when there is neither dissipation nor variation in crack propagation, the crack propagation energy is equal to the threshold which the tearing of the networks begins ( $G = G_0$ ). In such case, the applied total cutting energy  $G_{Total}$  was only offered by  $\Gamma_0 = 0.1 \text{ kJ/m}^2$  (see section 3.3), which frictional contribution equals to zero.  $\Gamma_0$  represents the minimum energy release rate to trigger the propagation of a crack.

#### 4. Discussions

The previous sections contain the results from the experiments together with the results from FE simulations of dynamic crack growth in rubber-like materials under conditions of steady-state. Tearing experiments indicate that there are two different fracture regimes related to the crack propagation velocity. The first regime A, at low deformation strain ( $\epsilon < 10\%$ ) (Fig. 7), the energy release rate  $\Gamma$  reached a plateau independent on the propagation velocity. The second regime B ( $\epsilon > 10\%$ ) (Fig. 7),  $\Gamma$  increases in a linear fashion with the velocity. This velocity-dependent is related to the dissipative mechanism of the linear viscoelastic fracture process. Gent and Shultz [28] and Andrews and Kinloch [29] showed that for elastomeric adhesives, the variations of the V-dependence of the fracture energy included a new dissipative factor (viscoelastic factor). Moreover, in studies where the effects of viscoelasticity on stretching are included (Kamasamudram et al. [30]), the limiting velocity depends on the glassy modulus of the material rather than the rubbery modulus. Therefore, the crack may exceed the velocity of the rubbery shear wave. Kamasamudram et al. [30] showed that when an elastomeric material is stretched and a crack is introduced, the crack propagates at a rate that depends on the initial stretch level. On the other hand, by increasing the stretch, this velocity exceeds the shear wave velocity based on the modulus of elasticity. In this case, the cracks can become faster due to the viscoelastic "stiffening" of the material.

Furthermore, As the stretch ratio increases in a sample of pure shear silicone, the rate of crack propagation increases. In this case, a hardening phenomenon occurs and the silicone becomes more tough. Long et al. [31] stated that, in tough gels, most of the energy release rate is dissipated and only a small fraction of it is used to drive the fracture process. Therefore, the amount of dissipation is strongly related to the local fracture process.

In the same case, Gzaïel et al. [23] showed that the increase of  $G_{fracture}$  can partially be caused by the viscoelastic dissipation term  $G_{viscoelastic}$  (V). Thus, the fracture energy therefore strongly depends on the applied velocity. As well as, it is significantly enhanced by this dissipative loss, which is larger than the intrinsic fracture energy (Gzaïel et al. [23]). Therefore, the fracture energy was assumed as the sum of the critical energy release rate (fracture energy at vanishing crack velocity), and the viscoelastic energy (velocity-dependent energy per unit crack surface created) dissipated during steady-state propagation at velocity V. Stress state of numerical tearing test was also assessed in this study by calculating the stresses involved during the crack propagation into an elastomeric membrane. The values of the stresses showed that the crack propagation was controlled by mixed fracture mode of mode I and mode II. The tension fracture Mode I was given by the tension stresses  $\sigma_{xx}$  and  $\sigma_{yy}$ , while the shear fracture Mode II was given by the shear stress  $\tau_{xy}$ . However, this increase is dominated by a uniaxial tension  $\sigma_{yy}$  (Fig. 11), which provides a fracture Mode I. Combined cutting and tearing experiments of silicone rubber using razor blade was conducted to set an experimental energy-based approach. Results show that the cutting force and the total cutting energy decreases significantly with increasing deformation ratio ( $4\% \leq \epsilon \leq 50\%$ ). As well, the tear energy only contributed to removing friction. Energy approach showed three different fracture regimes that related to the applied deformation:

First Part A (razor blade displacement = 10 mm): at  $\epsilon = 0\%$ , the maximum value of total cutting energy  $G_{Total}$  also partly encompasses frictional contribution of over 60%. Second Part (10 mm < razor blade displacement < 50 mm): When the applied stretch was increased ( $\epsilon \neq 0\%$ ), the frictional contribution decreased. During this step, the friction energy and the tear energy were both present during the cutting/tear test. The total cutting energy decreases significantly as the applied deformation increases, while the tear energy increases and the friction energy decreases more and more.

Third Part C (50 mm < razor blade displacement < 100 mm):  $G_{Total}$  decreased to reach a plateau leads to a constant value of  $0.1 \text{ kJ/m}^2$  since the increasing of the stretch. Results shown that  $G_{Total}$  seemed to be substantially unaffected with the applied deformation. Hence, it appears that the frictional contribution is completely removed starting from increasing of applied pre-strain ( $\epsilon \geq 5\%$ ).

This work proposes a numerical modeling approach validated through experiments to simulate cutting and tearing of silicone rubber. The results reveal two fracture regimes linked to crack propagation velocity, with viscoelastic mechanisms influencing the velocity dependence. Cutting and tearing experiments expose distinct regimes associated with applied deformation, highlighting the significant impact of friction. The primary objective of this study is to characterize the rupture mechanisms of silicone by combining experimental approaches and numerical modeling, providing a comprehensive understanding of material behavior under cutting and tearing conditions.

This research, focused on the cutting and tearing of soft materials, holds direct relevance for industries where stretchable elastomers are commonly used, including flexible electronics, wearable devices, soft robotics, and biomedical applications. The study provides valuable insights for engineers and designers in selecting elastomeric materials with favorable cutting and tearing



behaviors, enhancing the development of more resilient and durable products across various sectors. Furthermore, the findings contribute to the formulation of failure mitigation strategies by understanding the underlying mechanisms of cutting and tearing in elastomers. This knowledge enables the design and implementation of measures such as reinforcement, material composition adjustments, and optimization of manufacturing processes, thereby improving overall durability and reliability. In summary, the practical implications of this research extend beyond the laboratory, offering valuable perspectives for material selection and failure mitigation in applications involving stretchable elastomers, with the potential to significantly influence the design and development of a diverse range of products, enhancing their performance and longevity.

## 5. Conclusion

In summary, a computational framework for studying dynamic crack growth in rubber-like materials under conditions of steady-state has been proposed. The current work involves two parties, experimental and numerical, to investigate the mechanisms of dynamic fracture into silicone rubber. On the one hand, cutting test with stretching by sliding of blade and tearing test were carried out. On the other hand, a numerical simulation for the tearing test of pure shear sample was conducted using ABAQUS general static, assuming a nonlinear behavior silicone rubber-like material. The model accuracy was confirmed by comparing the obtained numerical results with the experimental ones.

The main purpose was to eliminate friction contribution and to study the contribution of viscoelastic dissipation of the total work of fracture required to propagate a crack in a rubber-like solid.

Firstly, we studied variation of energy release rate according to the crack propagation velocity. Average velocity of crack propagation ( $V$ ) was calculated dividing the variation in the position of the crack tip by time elapsed during this variation. Then, the energy balance developed by Zhu et al. [18] was used to measure the energy release rate  $\Gamma$ .

In that regard, the energy release rate has been shown to increase with propagation velocity.  $\Gamma(V)$  shows two fracture regimes, which is related to the applied strain deformation at low, and medium crack propagated velocities: Regime A (from 7% to 10%): The obtained values of  $\Gamma$  was noted  $\Gamma_0$ . And regime B (from 10% to 20%) in which we observed of the important viscoelasticity effects. Second, the numerical predicted and experimental values of average crack propagation velocity were consistent, suggesting that our XFEM can be used to investigate the mechanical fields and stress states. This method offers broad new possibilities in the understanding of fracture mechanisms in materials under large strain. Crack growth can be observed in a very general framework, involving dynamic, large strain, and material non-linearities. The use of XFEM during the loading phase of the sample provides the membrane displacement fields in which the crack will grow, and investigated the stress state. The stress analysis showed that tear tests of the silicone membrane display a mixed fracture mode, including two fracture modes (mode I and mode II). Finally, this work was conducted to set an experimental energy-based approach of combined cutting and tear test of silicone rubber using razor blade. Our results show that the cutting force and the total cutting energy decreases significantly with increasing deformation ratio ( $4\% \leq \epsilon \leq 50\%$ ). Moreover, the tear energy only contributed to removing friction, i.e., the crack becomes faster than the blade, which reduces the contact between the blade and the material.

Given that, for the further development of this study, we will carry out steady-state tests at high elongation (i.e., high speed) in order to investigate the fracture mechanism that will take place.

This initial work consists on XFEM-based modeling approach grounded in experimental investigations to study the cutting and tearing of soft materials. Overall, the results appear coherent and promising, showcasing the effectiveness of the XFEM approach in addressing these complex phenomena. However, it is crucial to underscore that the precision of the outcomes is sensitive to various numerical and experimental parameters. Key considerations include test conditions and the selection of boundary conditions. A thorough understanding of these parameters is essential for accurately interpreting the results and ensuring the reliability of the XFEM modeling. The nuances related to precision, contingent on these diverse factors, highlight the need for a meticulous approach in experimental design and numerical parameter tuning to guarantee a faithful representation of the cutting and tearing behavior of soft materials.

The correlation between tension and shear fractures, as well as the transition from stick-slip mode to regular propagation with increasing velocity, indeed prompts thorough consideration in the context of theory and prior studies. This phenomenon can be explored by examining the intricate interplay between tension and shear stresses, along with the viscoelastic mechanisms associated with crack propagation. Previous literature underscores the significance of viscoelastic behavior in elastomeric materials, potentially contributing to the observed transition. Furthermore, theoretical models like stick-slip have been investigated to comprehend shifts in crack propagation regimes. A comprehensive analysis of these theoretical concepts and their application in our study could shed light on the specific mechanisms governing these intricate fracture phenomena, paving the way for deeper understanding and future advancements in this field.

## Author Contributions

The manuscript was developed through the collaboration of all authors. Each of them contributed to the discussion of the results, reviewed, and approved the final version of the manuscript.

## Acknowledgments

The authors are thankful to Matteo Ciccotti and Frederic Lechenault (ESPCI Paris) for fruitful discussions.

## Conflict of Interest

There are no potential conflicts of interest concerning the research, authorship, and publication of this article.

## Funding

The authors received no financial support for the research, authorship, and publication of this article.

## Data Availability Statements

Not Applicable



## Nomenclature

$F_{cut}$	Cutting force	$G_{Total}$	Total cutting energy
$\lambda$	Elongation	$U_{Total}$	Total cutting work
$E$	Young modulus	$A$	Fracture surface
$\nu$	Poisson's ratio	$t$	Membrane thickness (mm)
$\rho$	Density	$x$	Razor blade displacement (mm)
$\Gamma$	Fracture energy	$V$	Crack propagation speed
$G_{rupture}$	Fracture energy	$\sigma_{xx}$	Tension stress
$\omega_0$	Width of the sample	$\sigma_{yy}$	Tension stress
$\sigma$	Cauchy stress tensor	$\tau_{xy}$	Shear stress
$\varepsilon$	Deformation strain	$G_{Fracture}$	Fracture energy
$I_1$	First invariant of the Cauchy strain tensor	$G_{Friction}$	Friction energy
$G_{cutting}$	Cutting energy	$G_{viscoelastic}$	Viscoelastic energy

## References

- [1] Rochow, E.G., INTRODUCTION A LA CHIMIE DES SILICONES, Dunod, Paris, 2ème édition, 1952.
- [2] Meunier, L., Chagnon G., Favier D., Orgéas L., Vacher P., Mechanical experimental characterisation and numerical modelling of an unfilled silicone rubber, *Polymer Testing*, 27, 2018, 765-777.
- [3] Corre, T., Rupture dynamique de membranes élastomères: étude expérimentale par mesure de champs, Diss. École centrale de Nantes, 2018.
- [4] Badr I., Frank H., Noel C., Comparison of the dimensional accuracy of one- and two-step techniques with the use of putty/wash addition silicone impression materials, *Materials Science*, 74, 1995, 535-541.
- [5] Chauvel, B., Turpin Y.-L., *Les matériaux à empreinte*, Université Médicale Virtuelle Francophone, 2010.
- [6] Bonsor S.J., Pearson G.J., *A Clinical Guide to Applied Dental Materials*, United Kingdom, Elsevier, 2013.
- [7] Lake, G.J., Yeoh, O.H., Measurement of rubber cutting resistance in the absence of friction, *International Journal of Fracture*, 14, 1978, 509-526, 1978.
- [8] Spagnoli, A., Terzano, M., Brighenti, R., Artoni, F., Stähle, P., The fracture mechanics in cutting: A comparative study on hard and soft polymeric materials, *International Journal of Mechanical Sciences*, 148, 2018, 554-564
- [9] Meunier, L., Chagnon G., Favier D., Orgéas L., *Experimental and Numerical Study of the Mechanical Behaviour of an Unfilled Silicone Rubber*, 5th European Conference on Constitutive Models for Rubber, ECCMR, Paris, France, 2007.
- [10] Baumberger, T., Caroli, C., Martina, D., Solvent control of crack dynamics in a reversible hydrogel, *Materials Letters*, 5, 2006, 552-555.
- [11] Baumberger, T., Caroli, C., Martina, D., Fracture of a biopolymer gel as a viscoplastic disentanglement process, *The European Physical Journal E*, 21, 2006, 81-89.
- [12] Triki, E., Combined puncture/cutting of elastomer membranes by pointed blades: an alternative approach of fracture energy, *Mechanics of Materials*, 97, 2016, 19-25.
- [13] Abaqus Documentation, Dassault Systèmes, 2017.
- [14] Gigliotti, L., *Assessment of the applicability of XFEM in Abaqus for modeling crack growth in rubber*, KTH School of Engineering Sciences, Department of Solid Mechanics, Royal Institute of Technology, Stockholm, Sweden, 2012.
- [15] Freund, L.B., *Dynamic Fracture Mechanics*, Cambridge University Press, 1998.
- [16] Griffith, A.A., The phenomena of fracture and flow in solids, *Philosophical Transaction of the Royal Society, Series A*, 221, 1921, 163-198.
- [17] Rivlin, R.S., Thomas, A.G., Fracture of rubber. I. Characteristic energy for tearing, *Journal of Applied Polymer Science*, 3, 1953, 291-318.
- [18] Zhu, Y., Luo, X., Ogden, R.W., Nonlinear axisymmetric deformations of an elastic tube under external pressure, *European Journal of Mechanics - A/Solids*, 29, 2009, 216.
- [19] Triki, E., Nguyen-Tri, P., Gauvin, C., Combined puncture and cutting of elastomer membranes: A fracture energy approach, *Journal of Applied Polymer Science*, 134, 2017, 44945.
- [20] Bouchbinder, E., Goldman, T., Fineberg, J., The dynamics of rapid fracture: instabilities, nonlinearities and length scales, *Reports on Progress in Physics*, 77(4), 2014, 046501.
- [21] Greensmith, H.W., Thomas, A., Fracture of rubber. iii. determination of tear properties, *Journal of Polymer Science Part A: Polymer Chemistry*, 1955, 18(88), 189-200.
- [22] Williams, M.L., Landel, R.F., Ferry, J.D., The temperature dependence of relaxation mechanisms in amorphous polymers and other glass-forming liquids, *Journal of the American Chemical Society*, 77(14), 1955, 3701-3707.
- [23] Gzaïel, M., Triki, E., Barkaoui, A., Chafra M., Finite element study of mixed fracture: velocity-dependent insertion of pointed blades into soft material, *International Journal of Applied Mechanics*, 13, 2021, 2150003.
- [24] Persson, B.N.J., Albohr, O., Heinrich, G., Ueba, H., Crack propagation in rubber-like materials, *Journal of Physics: Condensed Matter*, 17(44), 2005, R1071-R1142.
- [25] Stephenson, R.A., The equilibrium field near the tip of a crack for finite plane strain of incompressible elastic materials, *Journal of Elasticity*, 12, 1982, 65-99.
- [26] Vu-Khanh, T., Vu, T.B.N., Nguyen, C.T., Lara J., *Gants de protection: étude sur la résistance des gants aux agresseurs mécaniques multiples*, IRSST, Études et recherches, Rapport, 2005.
- [27] Triki, E., Nguyen-Tri, P., Gauvin, C., Azaiez, M., Vu-Khanh, T., Combined puncture/cutting of elastomer membranes by pointed blades: Characterization of mechanisms, *Journal of Applied Polymer Science*, 132(26), 2015, 42150.
- [28] Gent, A.N., Schultz, J., Effect of Wetting Liquids on the Strength of Adhesion of Viscoelastic Material, *The Journal of Adhesion*, 3(4), 1972, 281-294.
- [29] Andrews, E.H., Kinloch, A.J., Mechanics of adhesive failure. I, *Proceedings of the Royal Society A*, 27, 1973, 385-399
- [30] Kamasamudram, V., Coret, M., Moës, N., The role played by viscoelasticity in the bulk material during the propagation of a dynamic crack in elastomers, *International Journal of Fracture*, 231, 2021, 43-58.
- [31] Long, R., Hui, C., Fracture toughness of hydrogels: measurement and interpretation, *Soft Matter*, 12(39), 2016, 8069-8086.

## ORCID iD

Marwa Gzaïel  <https://orcid.org/0009-0000-1012-5956>

Ennouri Triki  <https://orcid.org/0009-0004-1203-1522>

Abdelwahed Barkaoui  <https://orcid.org/0000-0001-7268-5860>



© 2024 Shahid Chamran University of Ahvaz, Ahvaz, Iran. This article is an open access article distributed under the terms and conditions of the Creative Commons Attribution-NonCommercial 4.0 International (CC BY-NC 4.0 license) (<http://creativecommons.org/licenses/by-nc/4.0/>).



**How to cite this article:** Gzaiel M., Triki E., Barkaoui A. Experimental Study and Numerical Simulation of Cutting and Tearing of Silicone Rubber using Extended Finite Element Method, *J. Appl. Comput. Mech.*, 10(3), 2024, 465-478. <https://doi.org/10.22055/jacm.2024.45202.4327>

**Publisher's Note** Shahid Chamran University of Ahvaz remains neutral with regard to jurisdictional claims in published maps and institutional affiliations.

